

Improving Referring Image Segmentation using Vision-Aware Text Features

Hai Nguyen-Truong¹, E-Ro Nguyen^{2,3*}, Tuan-Anh Vu^{1†}, Minh-Triet Tran^{2,3},
Binh-Son Hua⁴, and Sai-Kit Yeung¹

¹ The Hong Kong University of Science and Technology

² University of Science, VNU-HCM, Ho Chi Minh City, Vietnam

³ Vietnam National University, Ho Chi Minh City, Vietnam

⁴ Trinity College Dublin, Ireland

Abstract. Referring image segmentation is a challenging task that involves generating pixel-wise segmentation masks based on natural language descriptions. Existing methods have relied mostly on visual features to generate the segmentation masks while treating text features as supporting components. This over-reliance on visual features can lead to suboptimal results, especially in complex scenarios where text prompts are ambiguous or context-dependent. To overcome these challenges, we present a novel framework VATEX to improve referring image segmentation by enhancing object and context understanding with Vision-Aware Text Feature. Our method involves using CLIP to derive a CLIP Prior that integrates an object-centric visual heatmap with text description, which can be used as the initial query in DETR-based architecture for the segmentation task. Furthermore, by observing that there are multiple ways to describe an instance in an image, we enforce feature similarity between text variations referring to the same visual input by two components: a novel Contextual Multimodal Decoder that turns text embeddings into vision-aware text features, and a Meaning Consistency Constraint to ensure further the coherent and consistent interpretation of language expressions with the context understanding obtained from the image. Our method achieves a significant performance improvement on three benchmark datasets RefCOCO, RefCOCO+ and G-Ref. Code is available at: https://nero1342.github.io/VATEX_RIS

Keywords: referring segmentation · vision-aware text features · CLIP localization · multimodal understanding · meaning consistency constraint

1 Introduction

Referring image segmentation (RIS) is an emerging new task in computer vision that predicts pixel-wise segmentation of visual objects in images from natural language cues. Compared to traditional segmentation [3, 14, 42, 44, 47, 49, 51], RIS

*Co-first author

†Corresponding author

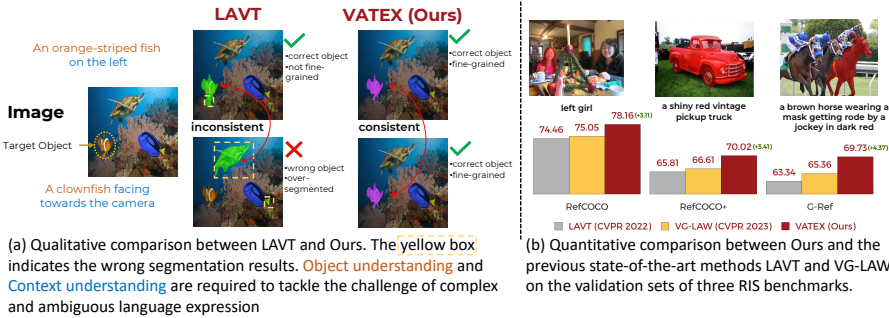


Fig. 1: VATEX outperforms previous state-of-the-art methods LAVT by utilizing vision-aware text features. Best view in zoom.

allows user-friendly interactions via text prompts to select and control the segmentation results, which is useful in various applications, especially interactive applications for image editing and robotics.

A particular technique to solve RIS is to obtain a robust alignment between language and vision. Performing such an alignment presents significant challenges due to the nature of languages, which are highly ambiguous and context-dependent. Early alignment approaches [11, 25, 35, 53] in RIS either used bottom-up methods, merging vision and language features in early fusion and using an FCN as a decoder to produce object masks, or top-down methods, which first identify objects in the image and use the expression as the grounding criterion to select the best-matched result.

Recent approaches [9, 30, 52] are based on transformers that learn the interaction between vision-text modalities followed by a standard encoder-decoder process to produce pixel-level segmentation results. However, this interaction still remains sufficiently underexplored in referring image segmentation. Specifically, the cross-modal interaction mainly occurs only in one way: keeping text features unchanged and utilizing them to enhance visual features. As a result, previous methods fail to identify the target object and generate precise segmentation for complex and challenging text expressions. For example, in Figure 1(a), although LAVT can easily segment the well-defined "orange-striped fish" and specific location information "on the left" in the first expression, LAVT struggles with the object "clownfish" and picks the turtle that is "facing towards the camera" in the second expression. We hypothesize that gradually putting the visual information into text features and performing the full bidirectional vision-text interactions can capture fine-grained semantic information of these modalities. This encourages us to focus more on vision-aware text features for object and context understanding.

First, for object understanding, we proposed integrating visual cues into text features in the query initialization process, facilitated by the visual-text embedding provided by CLIP [38]. We propose using the alignment between CLIP-Image and CLIP-Text embeddings to generate an *object-centric visual heatmap* that can be subsequently used as an initial mask for our model. By integrat-

ing this heatmap into the original text feature, we combine both linguistic and spatial information cues during the query initialization phase. This query initialization method transfers the knowledge from the pre-trained CLIP model and allows the model to localize the referred object correctly, even in the challenging case where the expression contains "unseen" category (*e.g.* clownfish).

Second, for context understanding, we introduce a Contextual Multimodal Decoder (CMD) to further exploit the superior interaction between visual and text modalities, especially the vision-to-language interaction. CMD aims to enhance text features by using contextual information obtained from the visual features and to bring the semantic-aware textual information back to visual features in a hierarchical architecture. While we can use the ground truth mask annotations as a direct learning signal to supervise the language-to-vision features, the opposite interaction is implicitly learned without any learning signal. By observing that there are multiple ways to describe an instance based on the context provided by the image, we propose the Meaning Consistency Constraint to enforce consistency of vision-aware text features across different expressions referring to the same instance in an image. The vision-to-language interaction can explicitly learn through this extra in-context learning signal, resulting in a *profound, coherent, and contextual understanding* in the feature space.

We present our novel framework **Vision-Aware TEXT** for Referring Image Segmentation (**VATEX**), which achieves superior performance on all splits of the RefCOCO, RefCOCO+, and G-Ref datasets, surpassing the current state of the art for each dataset by 3 – 4%. We also achieve state-of-the-art performance on both the validation split of Ref-YouTube-VOS and Ref-DAVIS 2017 with **65.4 $\mathcal{J}\&\mathcal{F}$** . Figure 1(b) demonstrates the differences in the complexity of the query sentences between three RIS benchmark datasets and the quantitative result of our proposed method compared to SOTA methods for RIS, which is LAVT [52] and VG-LAW [40]. In summary, our key contributions are as follows.

- We propose a novel DETR-based framework for referring image segmentation, specially designed to utilize vision-aware text features.
- We present a CLIP-based prior, a Contextual Multimodal Decoder, and a Meaning Consistency Constraint to address the complexities of cross-modal understanding and language ambiguities.
- Through extensive experiments on three referring image segmentation benchmarks (RefCOCO, RefCOCO+, G-Ref) and two referring video segmentation benchmarks (Ref-YouTube-VOS, Ref-DAVIS17), our approach sets the new state-of-the-art.

2 Related Work

Referring image segmentation [15] aims to generate pixel-wise segmentation masks for referred objects in images given a natural language expression. Early works [12, 16, 29] proposed to extract visual and linguistic features independently from convolutional and recurrent neural networks, respectively, and then concatenating these features to create multimodal features for decoding

final segmentation results. In recent works [1, 8, 10, 24, 52, 55], transformer-based multimodal encoders have been designed to fuse visual and text features, capturing the interaction between vision and language information in the early stage. VG-LAW [40] utilizes language-adaptive weights to dynamically adjust the visual backbone, enabling expression-specific feature extraction for better mask prediction while JMCELN [17] learns contextual embeddings and progressively aligns predictions for more accurate image segmentation. PolyFormer [30], on the other hand, treats this task as a sequential polygon generation process.

Query Initialization. The DETR (DEtection TRansformer) framework [2] has achieved impressive performance in object detection by directly transforming the task of object detection into a set prediction problem. Building upon DETR, several works have focused on improving the query initialization process for better performance. Deformable DETR [56] proposes a deformable transformer architecture to refine object queries, while DAB-DETR [31] directly uses the bounding box coordinate in the image to improve query initialization. In the field of referring segmentation, ReferFormer [46] extracts the word embeddings from the referring expression and treats them as the initial query for the framework. Our CLIP Prior elevates this approach by incorporating a CLIP-generated heatmap, enriching the textual features with spatial context during query initialization. This enriched query leads to improved performance in the subsequent segmentation stages.

Contrastive Learning is pivotal in advancing vision-language tasks [4, 5, 13, 48], enhancing model performance by distinguishing similarities and differences in visual and textual data. CLIP [38] employed a contrastive loss on an extensive image-text dataset. CRIS [45] leveraged text and pixel-level contrastive learning while VLT [9] applied masked contrastive learning to refine visual features across diverse expressions. Unlike previous approaches [9, 45] that solely focus on improving visual qualities by raw linguistic information, our work utilizes contrastive learning to enhance the comprehension of varied expressions conditioned in a shared image context before using it to enrich the visual features. This ensures the accuracy and stability of mutual interaction between text and visual features, particularly through the comparison of vision-aware expressions related to objects in an image.

3 Proposed Method

Our framework is constructed by three main components, as demonstrated in Figure 2. First, we propose a CLIP Prior module to generate an object-centric visual heatmap that localizes the object of interest from the text expression, which can be subsequently used to initialize the object queries for the DETR-based method (Section 3.1). Next, we propose to utilize cross-attention modules to interact between visual-text modalities in a hierarchical architecture via our Contextual Multimodal Decoder (Section 3.2). During training, we leverage Meaning Consistency Constraint to harness vision-aware text features generated by CMD to obtain a meaningful and consistent feature space (Section 3.3). We further adopt a

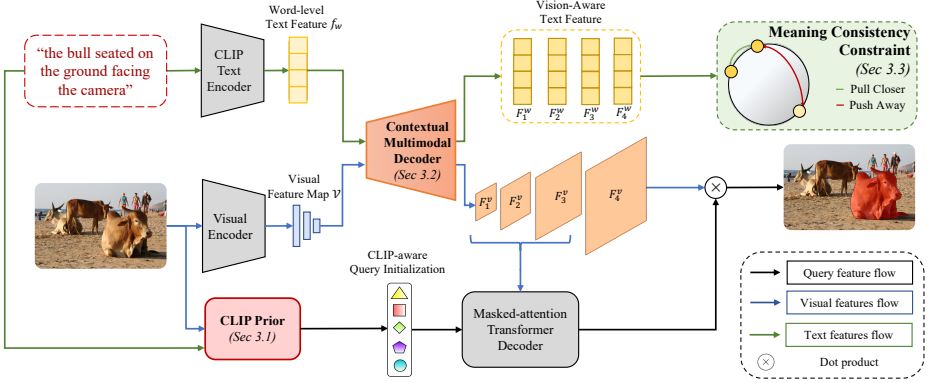


Fig. 2: The overall architecture of VATEX, which processes input images and language expressions through two concurrent pathways. Initially, the CLIP Prior module generates object queries, while simultaneously, traditional Visual and Text Encoders create multiscale visual feature maps and word-level text features. These visual and text features are passed into the Contextual Multimodal Decoder to enable multimodal interactions, yielding vision-aware text features and text-enhanced visual features. We then harness vision-aware text features to ensure semantic consistency across varied textual descriptions that reference the same object by employing sentence-level contrastive learning, as described in the Meaning Consistency Constraints section. On the other hand, the text-enhanced visual features and the object queries generated by the CLIP Prior are refined through a Masked-attention Transformer Decoder to produce the final output segmentation masks.

masked-attention transformer decoder [6] to enhance the object queries through multiscale text-guided visual features. Finally, the enhanced object queries and the visual features from CMD are utilized to output segmentation masks (Section 3.4).

Mathematically, given an input image with the size of $H \times W \times 3$, we can obtain the multiscale visual feature maps $\mathcal{V} = \{V_i\}_{i=1}^4$, $V_i \in \mathbb{R}^{H_i \times W_i \times C_i}$ from the Visual Encoder that captures the visual information in the data, where H_i, W_i, C_i denote the height, width, and the channel dimension of V_i . Given the L -word language expression as input, we use our Text Encoder to encode it into word-level text features $f_w \in \mathbb{R}^{L \times C}$ with C as the channel dimension. Our visual and text features will be further processed as described in the following sections.

3.1 Object Localization with CLIP Prior

To accurately locate the object of interest in the image from a text expression, it is essential to identify the visual region that is the most closely related to the expression. In previous work, query-based methods typically convert only *textual information* from the natural language into object queries [46] or learn the target object representation *implicitly* through multi-modal transformers [8]. Our goal is to leverage the exceptional alignment between *visual and text features* in the CLIP [38] model to generate the heatmap *explicitly* and embed that positional prior in the query.

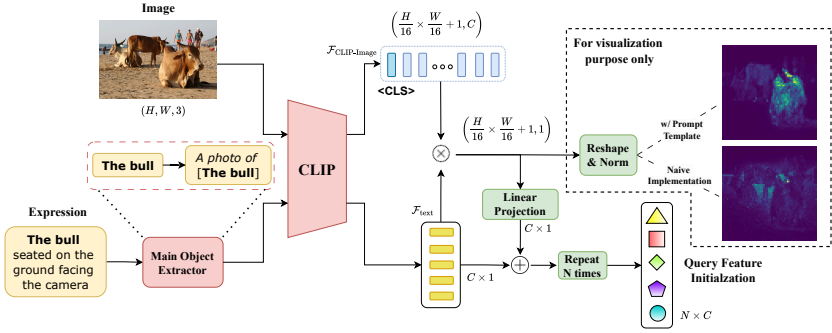


Fig. 3: Our CLIP Prior exploits the alignment of CLIP-Image and CLIP-Text embeddings for better query initialization. Best viewed with zoom.

A naive approach of entering full text expressions and images into the CLIP Model results in poor localization accuracy due to the **complex input sentence**. CLIP is trained to map textual descriptions to visual features, enabling it to identify various objects and visual concepts. Due to the diversity of these visual concepts, only a few specific features are activated for a particular class or category while the majority of features remain inactive and become redundant features. As the complexity of text prompts increases, there is a corresponding increase of redundant features within the feature space. When calculating the similarity between an image and a text query, these redundant features also contribute to the final output, causing noisy activations in the heatmap and degrading the model’s performance, as illustrated in Table 5. An example is provided in Figure 3 where the heatmap covers irrelevant regions in the image with spot activation and does not target to segment the main object of the sentence.

Additionally, the human approach to RIS does not involve parsing complex sentences entirely. Instead, we naturally break down a referring expression into its core components: the object of interest and its description with context information. Initially, the primary focus is on identifying what is the object mentioned in the expression (*e.g.* "the bull"). Following this, the search within the image is narrowed to objects that match the main object’s category. The final step involves using the specific characteristics or contextual information described in the expression to pinpoint the target object.

Inspired by this, we first extract the main noun phrase from the expression (*e.g.* the bull) in order to obtain a simplified text expression. Referring expressions in the RIS task are object-centric, which means that the main noun phrase can be considered as the main object of the sentence. We then convert the complex referring expression to a simple template-based sentence before passing it to the CLIP Encoder. In our implementation, we use "A Photo of [Object]" as our template as it is the most common prompt to describe an object [54] in CLIP, where the resulting text feature is represented by $\mathcal{F}_{\text{text}}$. We found that this improves the accuracy of the heatmap in localizing the object of interest.

In a separate flow, our input image goes through the CLIP Visual Encoder, resulting in features for multiple image tokens $\mathcal{F}_{\text{CLIP-Image}} \in \mathbb{R}^{(\frac{H}{16} \times \frac{W}{16} + 1) \times C}$.

While this template approach can efficiently localize regions of interest, it may lead to information loss due to oversimplification (*e.g.* focusing only on the bull in this scenario). However, its primary function is to narrow down the search space by *localizing a region* containing the object of interest, not necessarily finding out the exact object. To find the exact object of interest, the full-text expression needs to pass through the CMD and MCC for more comprehensive characteristics and contextual understanding.

Our visual heatmap for the object of interest can be obtained by calculating the similarity between the visual and text features, then reshaping to image space and going through L2-normalization:

$$\text{Heatmap} = \text{norm} \left(\frac{\mathcal{F}_{\text{CLIP-image}}}{\|\mathcal{F}_{\text{CLIP-image}}\|} \cdot \frac{\mathcal{F}_{\text{text}}}{\|\mathcal{F}_{\text{text}}\|} \right). \quad (1)$$

As normal practice, positional prior from CLIP is embedded to the text features by changing the dimension of the similarity map from $\frac{H}{16} \times \frac{W}{16} + 1$ to C , then repeat it N times together with the text features, then add these two to create initial object queries feature with N queries, each with C -dimension, for embedding the positional prior and text information into the query feature.

3.2 Contextual Multimodal Decoder

For a robust use of visual and text features in subsequent steps, we propose Contextual Multimodal Decoder (CMD) to produce multi-scale text-guided visual feature maps while enhancing contextual information from the image into word-level text features in a hierarchical design, see the architecture figure in the supplementary material. Specifically, our CMD is based on a feature pyramid network architecture [27], which has four levels. Each level transfers the semantic information from visual features to text features and then uses these vision-aware text features to update the visual features afterward via cross-modal attention.

In the i -th level of CMD, given the input visual features V_i and text features F_{i-1}^w , the multi-modal interactions are performed in two steps. First, a cross-attention that takes text features F_{i-1}^w as query and visual features V_i as key and value is used to model the relationship of the text and visual information. Then it forms the vision-aware text features by associating them with current text features:

$$F_i^w = \text{MHA}(F_{i-1}^w, V_i, V_i) \cdot F_{i-1}^w, \quad (2)$$

where $\text{MHA}(q, k, v)$ is the multi-head cross-attention module with query q , key k , value v .

F_i^w is then treated as the key and value and V_i is treated as the query in another multi-head cross-attention module to reinforce the alignment between the visual and text modalities and generate features V_i' . Consequently, V_i' is fused with the text-guided visual feature F_{i-1}^v from the previous level $i - 1$ followed

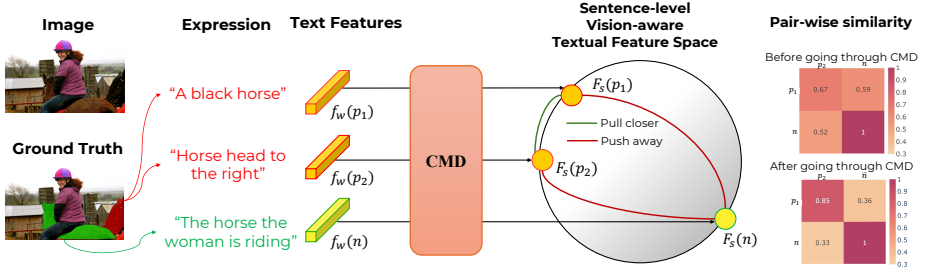


Fig. 4: Illustration of Meaning Consistency Constraint. Vision-aware text embeddings of different expressions are passed through a contrastive learning module in sentence-level feature space. Embeddings referring to the same object are pulled closer while pushing others far away. The cosine similarities of text features before and after CMD are shown on the right. Best view in color.

by a Conv2d layer to obtain the text-guided visual feature F_i^v . Mathematically, the whole process is as follows:

$$V'_i = \text{MHA}(V_i, F_i^w, F_i^w) \cdot V_i, \quad (3)$$

$$F_i^v = \text{Conv2d}(V'_i + \text{Ups}(F_{i-1}^v)), \quad (4)$$

where $\text{Conv2d}()$ is the 2D convolutional layer, and $\text{Ups}()$ denotes upsampling F_{i-1}^v to the size of V'_i . For the first level with $i = 1$, we skip F_0^v and let $F_0^w = f_w$, where f_w is the word-level linguistic features extracted by the Text Encoder.

3.3 Meaning Consistency Constraint

It is common for each object in an image to be described by different text expressions. Although the linguistic meaning of these descriptions may be different, they should convey the same semantic meaning when referencing that image (see two red expressions in Figure 4). According to this perspective, it's crucial for CMD to gradually comprehend contextual cues from visual features into textual representations and ensure consistent identification of target objects, where expressions referring to the same object yield identical representations. However, previous studies have often overlooked the relationship between expressions that pertain to the same instance.

To delve deeper into this relationship and provide the explicit in-context learning signal for vision-aware text features within CMD, we propose Meaning Consistency Constraint (MCC), a sentence-level contrastive learning approach. MCC aims to learn meaningful and discriminative representations for different expressions while consistently pulling sentences referring to the same object close to each other.

Unlike previous contrastive learning-based approaches [9, 45], we focus on linguistic features that are enriched and conditioned by visual information. This can encourage CMD module to gradually learn how to produce richer text features and lead to the improvement of visual features in context understanding due to the bidirectional attention mechanism and hierarchical design of CMD module.

Our contrastive learning pipeline is illustrated in Figure 4. During training, we construct a triplet of text expressions for each image. Each triplet comprises two sentences that refer to the same object (positive samples), along with a third sentence describing a different object (negative sample). We denote the positive samples by p_1, p_2 and the negative sample by n , respectively. With each sample x , we derive the sentence-level feature by averaging the vision-aware word-level textual features:

$$F_s(x) = \text{Avg}(F_4^w(x), \dim = 0), \quad (5)$$

where $F_4^w \in R^{L \times C}$, $F_s \in R^C$. We adopt the InfoNCE loss [37] to ensure that linguistic features referring to the same object converge, while features of different objects diverge:

$$\mathcal{L}_{mcc} = -\log \left(\frac{\text{sim}(p_1, p_2)}{\text{sim}(p_1, n) + \text{sim}(p_2, n)} \right), \quad (6)$$

where $\text{sim}(p, n) = \exp(F_s(p) \cdot F_s(n))$ to calculate the exponential for cosine similarity of sentence-level obtained from the text expressions.

3.4 Network Training

Prediction Heads. We adopt the masked-attention transformer decoder [6] to update our initial query feature f_o by using the multi-scale text-guided visual features $\{F_i^v\}_{i=1}^3$ to obtain the final object queries $F_o \in R^{N \times C}$. The final object queries will directly predict the probability of the target object $\hat{p} \in R^N$. The high-resolution segmentation mask $\hat{s} \in R^{\frac{H}{4} \times \frac{W}{4} \times N}$ is produced by associating between object queries F_o with the last fine-grained text-guided visual features $F_4^v \in R^{\frac{H}{4} \times \frac{W}{4} \times C}$, which can be formulated as:

$$\hat{s} = \text{Sigmoid}(F_4^v \cdot F_o^\top). \quad (7)$$

Instance Matching. The prediction set output from prediction heads is represented by $\hat{y} = \{\hat{y}_i\}_{i=1}^N$, where $\hat{y}_i = \{\hat{p}_i, \hat{s}_i\}$. Since a text expression refers to only a specific object, we denote the ground truth object as $y = \{p_{gt} = 1, s_{gt}\}$. The best prediction \hat{y}_δ can be found by a Hungarian algorithm [23] by minimizing the matching cost in terms of probability and segmentation mask [6, 7].

Training. Our prediction \hat{y}_δ is supervised by three losses. Firstly, the class loss \mathcal{L}_{cls} is binary cross entropy (BCE) loss to supervise the probability of referred object. Secondly, the mask loss \mathcal{L}_{mask} is a combination of dice loss and BCE. Finally, our sentence-level contrastive loss \mathcal{L}_{mcc} is used to enforce our Meaning Consistency Constraint. The total loss can be formulated as follows:

$$\mathcal{L}_{total} = \gamma_{cls}\mathcal{L}_{cls} + \gamma_{mask}\mathcal{L}_{mask} + \gamma_{mcc}\mathcal{L}_{mcc}, \quad (8)$$

where $\gamma_{cls}, \gamma_{mask}, \gamma_{mcc}$ are the scalar coefficients.

Inference. In inference, our method aligns with the standard practice of using a single image or video with one text expression, and MCC only requires sampling positive and negative expressions in the training phase. During inference, the query with the highest probability score is selected as the target object for the final output.

Table 1: Quantitative results of referring image segmentation on Ref-COCO, Ref-COCO+, G-Ref datasets on mIoU metric.

| Method | Backbone | | RefCOCO | | | RefCOCO+ | | | G-Ref | |
|---------------------|---------------|-------------|--------------|--------------|--------------|--------------|--------------|--------------|--------------|--------------|
| | Visual | Textual | val | testA | testB | val | testA | testB | val | test |
| VLT [8] | Darknet-53 | Bi-GRU | 65.65 | 68.29 | 62.73 | 55.50 | 59.20 | 49.36 | 52.09 | 56.65 |
| CRIS [45] | ResNet-101 | CLIP | 70.47 | 73.18 | 66.10 | 62.27 | 68.08 | 53.68 | 59.87 | 60.36 |
| CM-MaskSD [43] | CLIP-ViT-B | CLIP | 72.18 | 75.21 | 67.91 | 64.47 | 69.29 | 56.55 | 62.67 | 62.69 |
| LAVT [52] | Swin-B | BERT | 74.46 | 76.89 | 70.94 | 65.81 | 70.97 | 59.23 | 63.34 | 63.62 |
| JMCELN [17] | ResNet-101 | CLIP | 74.40 | 77.69 | 70.43 | 66.99 | 72.69 | 57.34 | 64.08 | 64.99 |
| VG-LAW [40] | ViT-B | BERT | 75.05 | 77.36 | 71.69 | 66.61 | 70.30 | 58.14 | 65.36 | 65.13 |
| VATEX (Ours) | Swin-B | CLIP | 78.16 | 79.64 | 75.64 | 70.02 | 74.41 | 62.52 | 69.73 | 70.58 |

Table 2: Quantitative results on video dataset using Video-Swin-B backbone.

| Methods | Ref-YT-VOS | | | Ref-DAVIS17 | | |
|---------------------|----------------------------|---------------|---------------|----------------------------|---------------|---------------|
| | $\mathcal{J}\&\mathcal{F}$ | \mathcal{J} | \mathcal{F} | $\mathcal{J}\&\mathcal{F}$ | \mathcal{J} | \mathcal{F} |
| ReferFormer [46] | 62.9 | 61.3 | 67.5 | 61.1 | 58.1 | 64.1 |
| VLT [9] | 63.8 | 61.9 | 65.6 | 61.6 | 58.9 | 64.3 |
| VATEX (Ours) | 65.4 | 63.3 | 67.5 | 65.4 | 62.3 | 68.5 |

Table 3: Performance comparison between LAVT and VATEX on Oc-IoU metric.

| Method | RefCOCO | RefCOCO+ | G-Ref |
|--------------|--------------|--------------|--------------|
| LAVT [52] | 62.51 | 50.79 | 56.01 |
| Ours w/o MCC | 66.42 | 54.92 | 59.25 |
| Ours | 68.20 | 57.38 | 61.69 |

4 Experimental Results

4.1 Experiment Setup

We evaluate the performance of our model on three image datasets: RefCOCO [18], RefCOCO+ [18], G-Ref [36] and further evaluate the performance of our model on two video datasets: Ref-Youtube-VOS [39] and Ref-DAVIS17 [19].

For evaluation metrics, we calculate mIoU to measure the overlap between the predicted segmentation mask and the ground truth mask for image segmentation. We also calculate region similarity \mathcal{J} and contour accuracy \mathcal{F} , and their average $\mathcal{J}\&\mathcal{F}$ for video object segmentation.

We use PyTorch to implement our method. During training, we freeze both the CLIP Visual and Text Encoder. Images are resized to a short side of 480. We set the coefficients for the losses as $\gamma_{cls} = 2$, $\gamma_{mask} = 5$, and $\gamma_{mcc} = 2$, with the feature dimension C set to 256. We train the network for 100,000 iterations on the RefCOCO(+g) datasets with an initial learning rate of 10^{-4} and is reduced by a factor of 0.1 at the 2/3 last iteration. For the Ref-Youtube-VOS dataset, we initialize the pre-trained weight from RefCOCO(+g) and train the network for 100,000 iterations. Regarding the Ref-DAVIS17 dataset, we directly use the weight obtained from the Ref-Youtube-VOS dataset for inference. For detailed information on each dataset and implementation, please see the supplementary material.

4.2 Main Results

Referring Image Segmentation. We compare our proposed method with the state-of-the-art methods on three common datasets (RefCOCO, RefCOCO+, G-Ref). As illustrated in Table 1, our method outperforms the state-of-the-art methods by a large margin in all splits of different datasets in the standard setting. Particularly, for the RefCOCO dataset, our method outperforms the recent

Table 4: Ablation Study on the val set of RefCOCO (mIoU) and Ref-YouTube-VOS ($\mathcal{J}\&\mathcal{F}$).

| CLIP Prior | CMD | MCC | RefCOCO | Ref-YT-VOS |
|------------|-----|-----|--------------------|------------------|
| - | - | - | 70.42 | 59.8 |
| ✓ | - | - | 71.95 +1.53 | 61.5 +1.7 |
| - | ✓ | - | 73.18 +2.76 | 61.9 +2.1 |
| - | ✓ | ✓ | 75.43 +5.01 | 63.6 +3.8 |
| ✓ | ✓ | ✓ | 78.16 +7.74 | 65.4 +5.6 |

Table 5: Analysis of prompt templates in CLIP Prior on RefCOCO validation set.

| Query Initialization method | RefCOCO (mIoU) |
|---|----------------|
| Text features as query [46] | 75.43 |
| CLIP Prior (Naive Implementation) | 74.34 -1.09 |
| CLIP Prior with Prompt "A Photo of [Object]" | 78.16 +2.73 |
| CLIP Prior mean's performance over 80 ImageNet prompts | 78.25 +2.82 |

VG-LAW, with mIoU gains of 3.11%, 2.28%, and 3.95% across the three splits, respectively. For the more complex RefCOCO+ dataset, our method outperforms the previous top method, JMCELN, by mIoU margins of 3.03%, 1.72%, and 5.18% in the validation, test A, and test B sets, respectively. The G-Ref dataset presented the most significant challenge, with longer and more complicated language expressions. Despite this, our method achieved remarkable performance improvements of approximately 5% in mIoU on the validation and test sets, compared to the second-best method, VG-LAW, in the same setting.

Referring Video Segmentation. Our model can be extended to video datasets with minor adaptations to handle temporal information. As shown in Table 2, VATEX outperforms the current SOTA methods VLT and ReferFormer on the same Video-Swin-B backbone by 1.6 and 3.8 $\mathcal{J}\&\mathcal{F}$ on the Ref-Youtube-VOS and Ref-DAVIS17 datasets, respectively.

4.3 More Analysis

Ablation Study. We conduct an ablation study on the validation sets of RefCOCO with Swin-B backbone and Ref-Youtube-VOS validation set with Video-Swin-B backbone to examine the impact of each proposed component in our model. The baseline follows the architecture of ReferFormer [46] by using only languages as the initial query (removing CLIP Prior), while only using text-guided vision features and ignoring the vision-aware text features (removing CMD and MCC). As shown in Table 4, the combination of CLIP Prior, CMD, and MCC modules results in the best performance, showcasing a remarkable performance increase of up to 7.74% in mIoU on RefCOCO and 5.6% in $\mathcal{J}\&\mathcal{F}$ on Ref-Youtube-VOS. This outcome unequivocally attests to the remarkable effectiveness of our approach and underscores its significant impact. The full ablation study is shown in the supplementary material.

CLIP Prior Analysis. As described in Section 3.1, our CLIP Prior relies on a template sentence to convert a complex sentence into a simplified sentence suitable for CLIP. The baseline which uses text features as initial query achieves 75.43% mIoU. We investigate the effects of using different templates and how these affect the final performance. Table 5 demonstrates that using the complex sentence leads to a significant deterioration in performance at 1.09%. In this case, CLIP introduces noisy activation on various objects based on their discriminative characteristics within the complex sentence, which is harmful to the model. By using the template "A Photo of [Object]", there is a notable improvement of 2.73% in mIoU. We conducted an additional experiment where we

aggregated the text embeddings from 80 ImageNet prompts, which has a very minor performance improvement. This demonstrates that the template “A Photo of [Object]” remains a practical choice.

Regarding the quality of the heatmap, Figure 1 demonstrates the enhanced localization performance achieved when prompt templates are utilized, compared to the original expression. Without simplifying the sentence, the heatmap tends to encompass distinctive categories in images or mentioned in the sentence (*e.g.* obstacles, woman and blue shirts), or highlights the wrong object (*e.g.* wind-surfing boat). By reducing the complexity of the text expression, it can be seen that the activation of the object of interest becomes more accurate. For more visualization, please see the supplementary material.

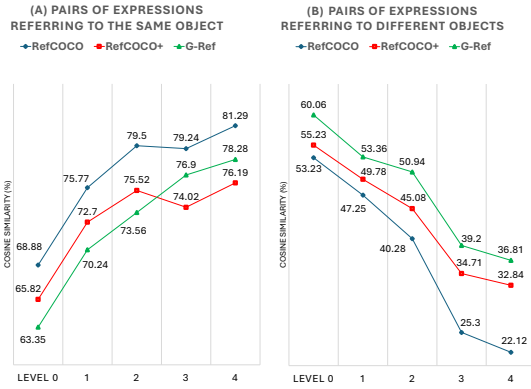


Fig. 5: Cosine similarities between sentence-level text features at each CMD level.

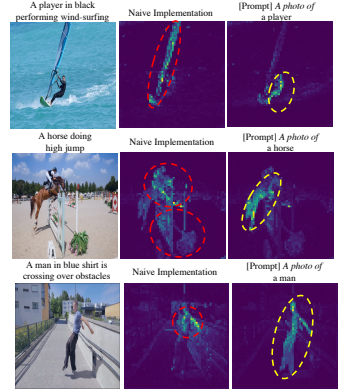


Fig. 6: Our heatmap from CLIP Prior.

Effect of CMD and MCC on Vision-aware Text Features. To study the impact of the CMD and MCC on text features, we calculate the similarity between sentence-level text features before and after processing through CMD. The average similarity results for all pairs of expressions referring to the same or different objects at each CMD level are depicted in Figure 5. Here, Level 0 represents the initial features, derived directly from the CLIP Embedding, while Level 4 indicates the final vision-aware text features of CMD.

In the context of expressions referring to the same object, the initial similarity of text features stands at 68.88%, 65.82%, and 63.35% for RefCOCO, RefCOCO+, and G-Ref, respectively. Following just one CMD level, the similarities witness an approximate 7% elevation across all datasets. The final vision-aware text features of the CMD process yield similarities of 81.29% in RefCOCO, 78.28% in RefCOCO+, and 76.19% in G-Ref.

Regarding different objects, we compute the similarity between all expressions pertaining to different objects within the same image to showcase the influence of our CMD module on them. As illustrated in Figure 5(b), the similarity between the features of these expressions progressively decreases from 53.23%, 55.23%, 60.06% to 22.12%, 32.82%, 36.81% on RefCOCO, RefCOCO+, and G-Ref, respectively.

These findings underscore the pivotal role of CMD in bolstering multimodal comprehension. Specifically, we reveal how CMD effectively improves the representation of text features that are conditioned on visual context, illustrating its significance in advancing the interaction between textual and visual information.

Effect of MCC on Object segmentation mask. To quantify the ability to consistently segment various expressions for the same object and further validate the effectiveness of our proposed Meaning Consistency Constraint, we leverage an Object-centric Intersection over Union (Oc-IoU) score, which calculates the overlap and union area between ground truth and all segmentation predictions of the same object. Specifically, consider the i -th object with K_i expressions referring to that object and the corresponding ground truth mask GT_i . Let P_i^j be the model's prediction for the j -th expression of the i -th object, where $j = 1..K_i$. The Object-centric IoU can be formulated as follows:

$$\text{Oc-IoU}(GT_i, P_i) = \frac{GT_i \cap P_i^1 \cap \dots \cap P_i^{K_i}}{GT_i \cup P_i^1 \cup \dots \cup P_i^{K_i}}, \quad (9)$$

$$\text{Oc-IoU}_{\text{total}} = \frac{1}{N} \sum_{i=1}^N \text{Oc-IoU}(GT_i, P_i), \quad (10)$$

where N is the total number of objects/instances in the datasets.

Table 3 provides the comparisons between our method and the state-of-the-art method LAVT in Oc-IoU on the validation set of three RIS benchmarks. As can be seen, our method outperforms LAVT in all three datasets. Comparing the last two rows of Table 3, we can see that the MCC helps the model, especially CMD to enhance mutual information between textual and visual features to further provide more consistent and accurate segmentation. These results underscore the compelling efficacy of our Meaning Consistency Constraint in resolving language ambiguities, thus improving the segmentation performance.

Qualitative Analysis. We provide the visualization of our results in Figure 7. Our method can successfully segment objects in complex scenarios, such as the presence of multiple similar objects. For example, in the first column, we can localize the guy who sits in the chair instead of the man standing on the tennis court. In the second sample, VATEX can distinguish the sushi plate among several food dishes that LAVT cannot. In the fourth column, our model can not only identify the correct umbrella belonging to the guy in the light jacket but also segment a part of the shaft of the umbrella that the ground truth does not provide. With the expression "bear child is hugging" in the sixth image, LAVT can only segment the bear's head, but VATEX can output the whole annotation of the target bear. However, our method fails to segment objects that need to be counted and selected by their order or be described indirectly through another object, as we have not leveraged counting information and object interaction in our model.

Another point worth mentioning is the differences in architecture design between VATEX and LAVT, with VATEX focusing on instance-based segmentation and LAVT on pixel-based segmentation. This will lead to smoother, more com-



Fig. 7: Results on RefCOCO(+/g) datasets. We compare our results with LAVT. Our method excels at segmenting objects in complex scenarios, such as distinguishing between similar objects and localizing specific instances within a scene. The last two columns of the results show failure cases. Best viewed in color.

plete segmentation masks by VATEX. However, this strength becomes a weakness when the model misidentifies an instance, resulting in entirely incorrect segmentation masks, whereas LAVT’s pixel-based approach can still partially identify the object in such situations.

5 Limitations and Future Works

Our method is not without limitations. Particularly, our method does not exploit the interaction and relationship between different objects as well as the alignment between actions and expressions referring to them (see Figure 7 the last two columns). Consequently, situations involving counting ("third from left"), indirect descriptions ("kid next to girl in pink pants"), or actions ("a woman walking to the left") might lead to inaccurate predictions. Dealing with intra-frame object relationships and inter-frame information is vital for future work. Another line of future work is making RIS work on general scenarios (*e.g.* segment all the red-colored objects, segment all the text in the image) or more fine-grained segmentation (*e.g.* segment the eye of the owl). It is also of great interest to investigate vision-aware text features with the SOTA vision-and-language model and to lift the referring expression segmentation task to the 3D domain.

6 Conclusion

This paper introduces VATEX, which examines how vision-aware text features can enhance the performance of RIS. First, we proposed adding visual cues to text features during the query initialization process in CLIP-Prior. Second, we exploit the interaction between visual-text modalities, especially in vision-to-language direction (CMD). Following that, we propose the MCC module

for maintaining a meaningful and consistent interpretation of various language phrases when referring to the same instance. In this approach, we take advantage of the dataset’s characteristic of containing multiple expressions for a single instance, a detail often overlooked by other methods. Looking ahead, we aim to bolster the robustness of MCC by enriching the diversity of language expressions through large Vision-Language Models (VLMs). Preliminary results demonstrating the use of VLMs to generate and augment expressions are detailed in the supplementary material, highlighting the promising direction of our research.

Improving Referring Image Segmentation using Vision-Aware Text Features – Supplementary Materials

Hai Nguyen-Truong¹, E-Ro Nguyen^{2,3*}, Tuan-Anh Vu^{1†}, Minh-Triet Tran^{2,3},
Binh-Son Hua⁴, and Sai-Kit Yeung¹

¹ The Hong Kong University of Science and Technology

² University of Science, VNU-HCM, Ho Chi Minh City, Vietnam

³ Vietnam National University, Ho Chi Minh City, Vietnam

⁴ Trinity College Dublin, Ireland

Our supplementary has 4 sections. Section 1 shows additional information about datasets and training procedure. Section 2 contains the additional experiments on RefCOCO(+g), Ref-Youtube-VOS and Ref-DAVIS17. This section also illustrates and analyzes the performance of CLIP Prior, CMD and MCC in different situations. Section 3 discusses about future work of VATEX, where we can enhance the expression’s diversity using GPT-4(V).

1 Additional Implementation Details

1.1 Datasets

Image datasets. RefCOCO and RefCOCO+ [18] are two of the largest image datasets used for referring image segmentation. They contain 142,209 and 141,564 language expressions describing objects in images. RefCOCO+ is considered to be more challenging than RefCOCO, as it focuses on purely appearance-based descriptions. G-Ref [36], or RefCOCOG, is another well-known dataset with 85,474 language expressions with more than 26,000 images. The language used in G-Ref is more complex and casual, with longer sentence lengths on average.

Video datasets. Ref-YouTube-VOS [39] and Ref-DAVIS17 [19] are well-known datasets for referring video object segmentation. Ref-YouTube-VOS contains 3978 video sequences with approximately 15000 referring expressions, while Ref-DAVIS17 consists of 90 high-quality video sequences. These datasets are used to evaluate the performance of algorithms that aim to identify a specific object within a video sequence based on natural language expressions.

1.2 Training Details

Our model is optimized using AdamW [34] optimizer with the initial learning rate of 10^{-5} for the visual encoder and 10^{-4} for the rest. Our model comprises a total

*Co-first author

†Corresponding author

Table 1: Fair Backbone Comparison between CRIS, JMCELN, LAVT and VATEX.

| Method | Backbone | | RefCOCO | | |
|---------------------|------------|---------|--------------|--------------|--------------|
| | Visual | Textual | val | testA | testB |
| CRIS [45] | ResNet-101 | CLIP | 70.47 | 73.18 | 66.10 |
| JMCELN [17] | ResNet-101 | CLIP | 74.40 | 77.69 | 70.43 |
| VATEX (Ours) | ResNet-101 | CLIP | 75.66 | 77.88 | 72.36 |
| LAVT [52] | Swin-B | BERT | 74.46 | 76.89 | 70.94 |
| LAVT [52] | Swin-B | CLIP | 73.15 | 75.24 | 70.02 |
| VATEX (Ours) | Swin-B | CLIP | 78.16 | 79.64 | 75.64 |

Table 2: Precision analysis at different threshold value comparison between VATEX and recent SOTA methods.

| Methods | Pr@0.5 | Pr@0.7 | Pr@0.9 | mIoU |
|----------------|--------|--------|--------|-------|
| LAVT [52] | 84.46 | 75.28 | 34.30 | 74.46 |
| ReLA [28] | 85.92 | 77.71 | 34.99 | 75.61 |
| CG-Former [41] | 87.23 | 78.69 | 38.77 | 76.93 |
| VATEX | 88.12 | 82.54 | 45.11 | 78.17 |

of nine Masked-Attention Transformer Decoder layers followed [6]. We set the number of queries to 5 [46]. For the setting of training from classification weight from Imagenet on Ref-Youtube-VOS dataset, we train the model for 200,000 iteration with the learning drop at 140,000-th iteration. On Ref-DAVIS17 [19], we directly report the results using the model trained on Ref-YouTube-VOS without finetuning.

2 Additional Quantitative Results and Analysis

2.1 Additional Comparison on RefCOCO(+/g)

Fair backbone Comparison. We have benchmarked our model, VATEX, using the ResNet-101 backbone, aligning it with CRIS and JMCELN for a more equitable comparison. This adaptation demonstrates VATEX’s superior performance, achieving a 1.26% improvement on RefCOCO val and a significant 1.93% on RefCOCO testB over the current state-of-the-art methods.

Further, to address comparisons with LAVT, we have experimented with CLIP as the text encoder, adhering to the official repository guidelines. This experiment revealed a performance decline of approximately 1% when substituting BERT with CLIP as the text encoder. This finding underscores the critical importance of using the CLIP Image Encoder together with the CLIP Text Encoder to maintain model performance. A similar trend was observed with ReferFormer, reinforcing our conclusion. Consequently, when compared to LAVT under the fair conditions in backbone, VATEX shows a substantial improvement, outperforming by 5.01%, 4.40%, and 5.62% on RefCOCO val, testA, and testB, respectively. This data confirms the effectiveness of our approach and the importance of consistent backbone usage for fair and accurate performance assessment.

Precision Analysis Table 2 presents a detailed comparison between our model, VATEX, and other leading methods such as LAVT, ReLA, and CG-Former, highlighting VATEX’s remarkable superiority across benchmarks, particularly in Pr@0.7 and Pr@0.9. Notably, VATEX exceeds CG-Former by 6.34% and ReLA by 10.12% at the Pr@0.9 benchmark, showcasing its exceptional ability to achieve complete and accurate segmentation of different instances within images. This performance is evidenced by its high precision scores, as well as through visualizations. To further enhance VATEX’s mIoU, an improved matching function is

Table 3: Quantitative results of referring image segmentation on Ref-COCO, Ref-COCO+, G-Ref datasets with other SOTA methods using external training data. VATEX is trained with Swin-B backbone

| Method | Datasets used | RefCOCO | | | RefCOCO+ | | | G-Ref | |
|---------------------------------|---------------------------|--------------|--------------|--------------|--------------|--------------|--------------|--------------|-------------|
| | | val | testA | testB | val | testA | testB | val | test |
| SeqTR [55] | Visual Genome (5.4M) | 71.7 | 73.31 | 69.82 | 63.04 | 66.73 | 58.97 | 64.69 | 65.74 |
| RefTR [24] | Flickr30k-entities (158K) | 74.34 | 76.77 | 70.87 | 66.75 | 70.58 | 59.4 | 66.63 | 67.39 |
| PolyFormer-B [30] | RefCOCO(+g) (368K) | 75.96 | 77.09 | 73.22 | 70.65 | 74.51 | 64.64 | 69.36 | 69.88 |
| VATEX_{RefCOCO} | RefCOCO (142K) | 78.16 | 79.64 | 75.64 | - | - | - | - | - |
| VATEX_{RefCOCO+} | RefCOCO+ (141K) | - | - | - | 70.02 | 74.41 | 62.52 | - | - |
| VATEX_{G-Ref} | G-Ref (85K) | - | - | - | - | - | - | 69.73 | 70.58 |
| VATEX_{joint} | RefCOCO(+g) (368K) | 81.53 | 82.75 | 79.66 | 74.61 | 78.75 | 68.52 | 75.54 | 76.4 |

Table 4: Quantitative results of referring image segmentation on Ref-COCO, Ref-COCO+, G-Ref validation datasets with SOTA vision foundation models.

| Method | RefCOCO | RefCOCO+ | G-Ref |
|------------------------------|--------------|--------------|--------------|
| Grounded-SAM [32] [22] | 67.19 | 58.96 | 59.14 |
| X-Decoder [57] | - | - | 67.5 |
| SEEM [58] | - | - | 67.8 |
| VATEX | 78.16 | 70.02 | 69.73 |
| VATEX_{joint} | 81.53 | 74.61 | 75.54 |

essential for precisely aligning instances with user expressions, underscoring our next steps in improving VATEX’s performance in the future.

External/Multiple Training dataset SeqTR, RefTR, and PolyFormer enhance their performance on the RefCOCO dataset by incorporating external datasets—Visual Genome with 5.4M descriptions across over 33K categories, Flickr30k-entities with 158K descriptions, and the joint dataset RefCOCO(+g) with 368K descriptions. Their papers indicate that using such external datasets for pretraining can improve performance by 8-10%.

Compared to PolyFormer [30], without using external pretraining dataset, VATEX_{RefCOCO} demonstrates superior performance over PolyFormer-B, while VATEX_{RefCOCO+} and VATEX_{G-Ref} achieve comparable results with [30] while using **42x** and **69x** smaller datasets respectively, with the exception of the RefCOCO+ test B. The performance’s gap on RefCOCO+ Test B, which focuses on non-human objects described purely by their appearance (*e.g.* "the porcelain throne," "part of the bed occupied by a black pamphlet"), could be attributed to the varied object categories covered during the pre-training phase with extensive external datasets.

On the otherhand, VATEX_{joint} adopts a different strategy. By solely utilizing the RefCOCO(+g) dataset, which is **16x smaller** than the datasets used by PolyFormer, VATEX_{joint} with Swin-B backbone still achieves remarkable results. Specifically, VATEX_{joint} outperforms PolyFormer by 4-6% across all benchmarks, setting a new state-of-the-art result on the RefCOCO dataset.

Comparison with SOTA vision foundation models Table 4 illustrates the quantitative performance between VATEX with generalist foundation models: Grounded-SAM [32] [22], SEEM [58] and X-Decoder [57] in Table 4. For Grounded-SAM, we first use Grounding DINO to extract the bounding box prediction from the text prompt, then we feed that bounding box to SAM to obtain the final segmentation mask. For X-Decoder and SEEM, we directly use the report number on their official github[†] with Focal-L backbones. While VATEX is trained on much smaller dataset sizes and smaller backbones, VATEX_{joint} still significantly outperforms Grounded-SAM with 14.34%, 15.65%, and 16.4% improvements on RefCOCO, RefCOCO+ and G-Ref, respectively. Compared with X-Decoder and SAM, which are trained and finetuned on RefCOCO(+/g) datasets, we also outperform them with approximately 2% with VATEX and 7.7% with VATEX_{joint},

2.2 Experimental Results on Ref-YoutubeVOS and Ref-DAVIS17

The result for Ref-Youtube-VOS dataset is shown in Table 5. As can be seen, our method demonstrates superior performance, setting a new state-of-the-art for referring video object segmentation on the Ref-Youtube-VOS dataset with different backbones. In particular, our approach with the spatial-temporal backbone (e.g., Video-Swin [33]) and pre-trained weights from the image dataset achieves the highest $\mathcal{J}\&\mathcal{F}$ score of 65.4% among all other methods on the Ref-Youtube-VOS dataset, including VLT and ReferFormer.

Table 5: Comparison with the SOTA on Ref-Youtube-VOS.

| Methods | Backbone | Ref-Youtube-VOS | | |
|---|---------------------|----------------------------|---------------|---------------|
| | | $\mathcal{J}\&\mathcal{F}$ | \mathcal{J} | \mathcal{F} |
| Train with Image segmentation weight from RefCOCO(+ /g) | | | | |
| ReferFormer [46] | ResNet-50 | 55.6 | 54.8 | 58.4 |
| RR-VOS [26] | ResNet-50 | 57.3 | 56.1 | 58.4 |
| VATEX (Ours) | ResNet-50 | 58.5 | 57.1 | 59.9 |
| ReferFormer [46] | Swin-L | 62.4 | 60.8 | 64.0 |
| VATEX (Ours) | Swin-L | 64.2 | 61.4 | 67.0 |
| ReferFormer [46] | Video-Swin-B | 62.9 | 61.3 | 64.6 |
| VLT [9] | Video-Swin-B | 63.8 | 61.9 | 65.6 |
| VATEX (Ours) | Video-Swin-B | 65.4 | 63.3 | 67.5 |

Table 6: Quantitative results of referring video object segmentation on Ref-DAVIS17.

| Methods | Backbone | Ref-DAVIS17 | | |
|---------------------|---------------------|----------------------------|---------------|---------------|
| | | $\mathcal{J}\&\mathcal{F}$ | \mathcal{J} | \mathcal{F} |
| ReferFormer [46] | ResNet-50 | 58.5 | 55.8 | 61.3 |
| RR-VOS [26] | ResNet-50 | 59.7 | 57.2 | 62.4 |
| VATEX (Ours) | ResNet-50 | 61.2 | 58.2 | 64.3 |
| ReferFormer [46] | Video-Swin-B | 61.1 | 58.1 | 64.1 |
| VLT [9] | Video-Swin-B | 61.6 | 58.9 | 64.3 |
| VATEX (Ours) | Video-Swin-B | 65.4 | 62.3 | 68.5 |

The results for Ref-DAVIS17 are shown in Table 6. Similarly, our approach achieves competitive performance compared to other state-of-the-art methods in referring video object segmentation. Specifically, with backbones ResNet-50, our proposed model outperforms ReferForme and achieves slightly better results than RRVOS. Moreover, our method achieves the best performance among all methods with the Video-Swin-B backbone with a $\mathcal{J}\&\mathcal{F}$ score of 65.4%, which is 3.8% higher than the closest competitor VLT.

[†]<https://github.com/UX-Decoder/Segment-Everything-Everywhere-All-At-Once/>



Fig. 1: Our heatmap from CLIP Prior. By reducing the complexity of the text expression, it can be seen that the activation on the object of interest becomes more accurate. Best view in zoom.

2.3 Heatmap of CLIP Prior

To obtain the heatmap result, from the vector of shape $(\frac{H}{16} \times \frac{W}{16} + 1, 1)$, we remove "CLS" token and reshape it into 2D heatmap of $\frac{H}{16} \times \frac{W}{16}$. For visualization purposes, we resize the original image to 960×960 , then pass it through CLIP-Image Encoder, resulting in a high-quality heatmap of size 60×60 . Notably, we only use a default input size of 224×224 during training. Regarding the quality of the heatmap, Figure 1 demonstrates the comparison between the naive implementation and our prompt-based template. In the 3rd and 7th rows, it is evident that simplifying the sentence and employing prompt templates can aid in distinguishing the target object from the image, resulting in decreased localization errors.

While CLIP Prior excels at localizing objects of interest, it can struggle in complex cases where the expression describes multiple instances within the same category and their relative positions (*e.g.* bottom right of Figure 1). In these situations, the heatmap may encompass all objects within the category rather than the specific referred instances. However, CLIP Prior’s core purpose is to narrow down the relevant region, not pinpoint the exact object. Identifying the precise instance will be handled later in the full-text prompt by the Transformer architecture, which can leverage additional context and relationships.

Moreover, CLIP Prior can also help the model in cases when the referring expression contains out-of-vocabulary objects. By transferring the knowledge from CLIP and embedding the heatmap into the query initialization, the model can obtain a good segmentation mask based on the cues from CLIP Prior. Figure 2 shows how CLIP Prior heatmap can help the model to localize the object in the early phase, thus improving the model’s performance.

2.4 Computational analysis of CLIP-Prior

It is easy to implement and incorporate CLIP Prior into query-based segmentation model. With CLIP-based models the heatmap can be generated without any additional computational cost through matrix multiplication and L2-normalization, as illustrated in Equation 1. For non-CLIP-based models like

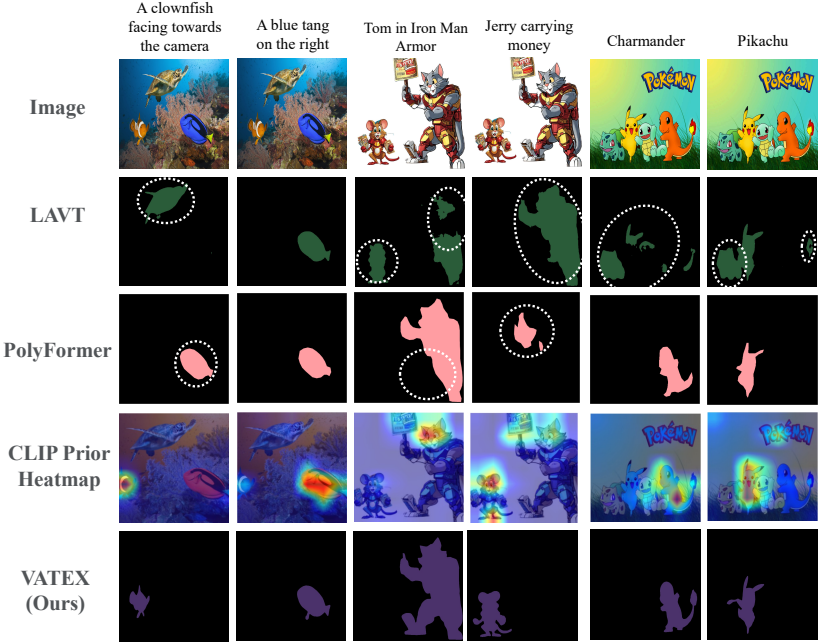


Fig. 2: Comparison between VATEX with SOTA methods on some hard cases of referring image segmentation. By using the CLIP Prior heatmap, our VATEX can segment the correct objects in hard vocabulary situation.

ReLA [28], the BERT text encoder needs to be replaced with the CLIP-Text Encoder, and an additional CLIP-Image Encoder is employed to obtain the well aligned embeddings from the CLIP Model. The overall computational cost for ReLA, measured in FLOPS, is calculated as:

$$\begin{aligned} \text{FLOPS}(\text{ReLA w/ CLIP Prior}) = & \text{FLOPS}(\text{ReLA w/o CLIP Prior}) \\ & - \text{FLOPS}(\text{BERT}) + \text{FLOPS}(\text{CLIP}), \end{aligned}$$

with $\text{FLOPS}(\text{BERT}) \approx 3.42 \text{ GFLOPS}$ and $\text{FLOPS}(\text{CLIP}) \approx 10.24 \text{ GFLOPS}$ for a 20-word sentence and an 224×224 image.

2.5 Comparison between VATEX with and without CLIP Prior and other methods

CLIP-based model in RIS. Adopting CLIP is a good practice taken by several previous methods, including CRIS, CM-MaskSD, and RIS-CLIP. However, to effectively use the aligned embedding from CLIP to obtain good results in referring segmentation is an open question. For example, although using powerful CLIP as the backbone, the SOTA CLIP-based method RIS-CLIP [21] has a comparable performance with the SOTA Non-CLIP model VG-LAW [40]. To analyze it, we take CRIS [45] as a baseline for CLIP-based model. CRIS directly

Table 7: Quantitative results of referring image segmentation on Ref-COCO, Ref-COCO+, G-Ref validation datasets on CLIP-based and Non-CLIP model.

| Method | RefCOCO | RefCOCO+ | G-Ref |
|-------------------------|--------------|--------------|--------------|
| CLIP-based Model | | | |
| CRIS [45] | 70.47 | 62.27 | 59.87 |
| CM-MaskSD [43] | 72.18 | 64.47 | 62.67 |
| RIS-CLIP [21] | 75.68 | 69.16 | 67.62 |
| Ours w/ CLIP Prior | 78.16 | 70.02 | 69.73 |
| Non-CLIP Model | | | |
| LAVT [52] | 74.46 | 65.81 | 63.34 |
| VG-LAW [40] | 75.05 | 66.61 | 65.36 |
| Ours w/o CLIP Prior | 75.43 | 67.38 | 68.12 |

used the well-aligned embedding space between text and vision for RIS. However, the performance of this work is not good compared to others, as there are two concerns with relying solely on CLIP for referring image segmentation tasks:

1. Frozen CLIP Model. CLIP model, trained on object-centric images, generates visual features focusing on semantic class meanings rather than instance-based details (see bird example in Figure 1). This limits the effectiveness of CLIP for instance-level tasks.
2. Fine-tuning CLIP Model. Fine-tuning the CLIP model risks overfitting on training samples, thereby diminishing its ability to generalize features to novel classes.

We found that learning from a visual backbone pre-trained on ImageNet and only utilizing frozen CLIP as a prior gave better performance on both instance-level segmentation and open-vocabulary segmentation nature of RIS.

For a truly fair comparison, we provide our method w/o CLIP, which achieves 75.43, 67.38, and 68.12 mIoU, and we still outperform the SOTA LAVT (74.46, 65.81, and 63.34) and VG-LAW (75.05, 66.61 and 65.36) on RefCOCO(+/g) in the same setting.

2.6 Full ablation study

Table 8 presents an ablation study conducted on the validation set of RefCOCO and Ref-Youtube-VOS, evaluating the mIoU (mean Intersection over Union) and $\mathcal{J}\&\mathcal{F}$, respectively of different model configurations. The study explores the impact of three components: CLIP Prior, CMD (Contextual Multimodal Decoder), and MCC (Meaning Consistency Constraint).

The first row represents the baseline model with none of the studied components incorporated. The mIoU for this configuration is 70.42% mIoU and 59.8 $\mathcal{J}\&\mathcal{F}$. In rows 2 to 4, the ablation study reveals that incorporating independently the CLIP Prior alone (row 2) and CMD (row 3) both contribute positively to the mIoU on the RefCOCO and $\mathcal{J}\&\mathcal{F}$ on Ref-YoutubeVOS validation set with

Table 8: Ablation Study on the validation set of RefCOCO (mIoU) and Ref-Youtube-VOS ($\mathcal{J}\&\mathcal{F}$).

| | CLIP Prior | CMD | MCC | RefCOCO | Ref-Youtube-VOS |
|---|------------|-----|-----|---------------|-----------------|
| 1 | - | - | - | 70.42 | 59.8 |
| 2 | ✓ | - | - | 71.95 $+1.53$ | 61.5 $+1.7$ |
| 3 | - | ✓ | - | 73.18 $+2.76$ | 61.9 $+2.1$ |
| 4 | - | - | ✓ | 70.70 $+0.30$ | 60.2 $+0.4$ |
| 5 | ✓ | ✓ | - | 75.12 $+4.72$ | 63.1 $+3.3$ |
| 6 | ✓ | - | ✓ | 72.14 $+1.74$ | 61.3 $+1.5$ |
| 7 | - | ✓ | ✓ | 75.43 $+5.01$ | 63.6 $+3.8$ |
| 8 | ✓ | ✓ | ✓ | 78.16 $+7.74$ | 65.4 $+5.6$ |

an improvement of 1.53%, 2.76% mIoU and 1.7%, 2.1% $\mathcal{J}\&\mathcal{F}$, whereas the introduction of the Meaning Consistency Constraint (MCC) alone (row 4) leads to a modest increase (only 0.30% mIoU and 0.4 $\mathcal{J}\&\mathcal{F}$), emphasizing the individual significance of each component in enhancing model performance. Although MCC alone has a modest impact, when combined with the CMD in row 7, there is a notable improvement of 4.7% (mIoU of 75.1) and 3.3% ($\mathcal{J}\&\mathcal{F}$ of 63.1). This synergy demonstrates that while MCC alone may not perform exceptionally, its collaboration with CMD effectively enhances model performance, aligning with our approach of leveraging enriched text features conditioned by visual information for improved mutual interaction. The final row represents the model with all components (CLIP Prior, CMD, and MCC) combined, achieving the highest mIoU of 78.16 ($+7.74$) and $\mathcal{J}\&\mathcal{F}$ of 65.4 ($+5.6$).

2.7 More on Contextual Multimodal Decoder and Meaning Consistency Constraint

Architecture Figure of CMD For a robust use of visual and text features in subsequent steps, we propose to fuse visual and text features using a Contextual Multimodal Decoder (CMD), which is designed to produce multi-scale text-guided visual feature maps while enhancing contextual information from the image into word-level text features in a hierarchical design as shown in Figure 3. The process on each level of CMD is achieved by a Bi-directional Attention Transfer(BAT), which incorporates two cross-attention modules.

2.8 Length of language expressions

In Figure 4, we provide a detailed analysis of the performance of our approach based on the length of language expressions. To do this, we followed the approach in [20] and split each validation set of the dataset into four groups based on the length of the language expressions (sentence length), with each group being roughly the same size. Our approach VATEX achieved outstanding results, outperforming most previous methods with large margins of over 4% in IoU, except for the group of length 6-7 on RefCOCO, where the difference in performance was only 0.5%. Notably, our approach demonstrated exceptional

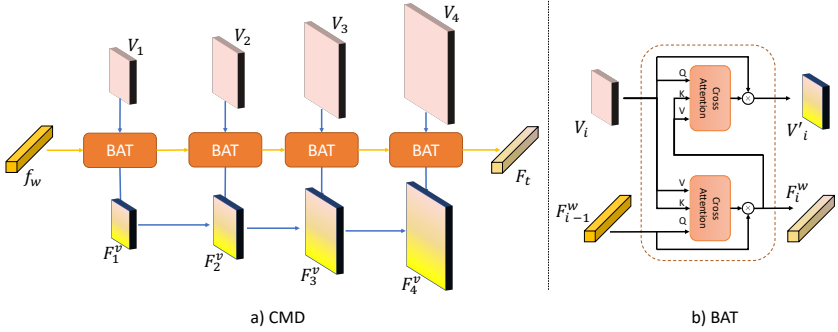


Fig. 3: The architecture of Contextual Multimodal Decoder.

performance on the G-Ref dataset, surpassing the previous methods [20] by a remarkable margin of more than 10% on each sentence length group. These results attest to the effectiveness of our approach in handling the challenges posed by diverse and complex referring expressions in the G-Ref dataset. Additionally, our approach displayed less performance deterioration across the range of sentence lengths on three datasets compared to others. Our findings suggest that our approach accurately identifies objects in complex and diverse visual scenes, rendering it a promising solution for real-world applications where accurate and efficient segmentation is crucial.

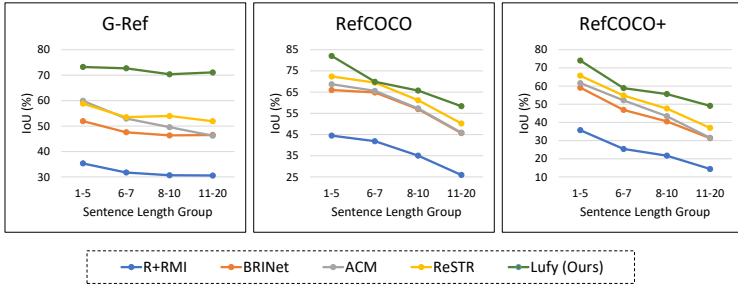


Fig. 4: Performance in IoU versus sentence length group on three referring image datasets.

3 Enhancing Expression Diversity in Referring Image Segmentation Datasets through Prompting Techniques

Our method’s utilization of diverse referring expressions for each object aligns with established best practices in text-image dataset annotation. This approach is widely accepted and implemented across several benchmark datasets. In scenarios where multiple expressions per object are unavailable, we have the flexibility to employ Large Language Models (LLMs) for enhancing expression diversity.

This can be achieved either by augmenting existing expressions or generating new ones based on object masks, a technique successfully employed by datasets like RIS-CQ. Furthermore, we demonstrate a practical application of this approach through a sample that showcases how we can prompt ChatGPT to generate relevant expressions in Fig. 5. This generation is based on factors like an object’s position in the image, its relative position to other objects or people, and distinguishing attributes such as color or appearance.

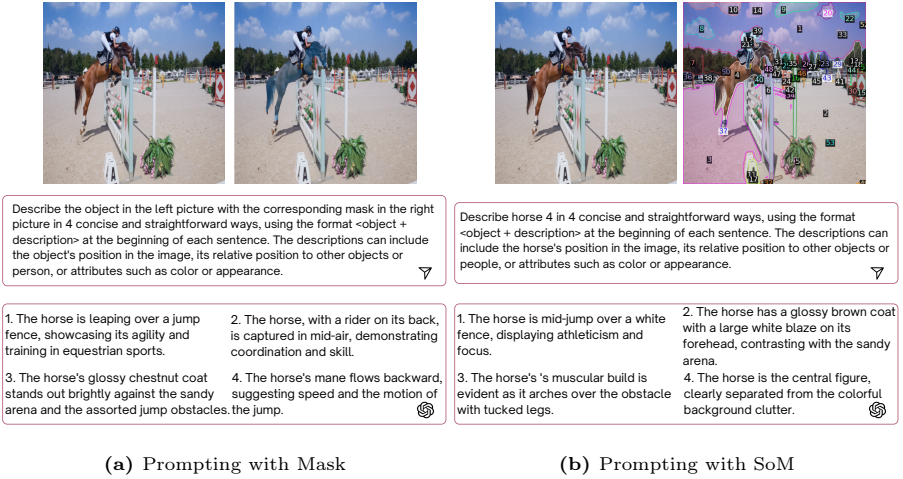


Fig. 5: Example of using GPT-4(V) with different prompting techniques to generate object description.

Figure 10 showcases two innovative prompting techniques for generating object descriptions. On the left, we demonstrate how combining an original image with its masked version can effectively prompt GPT-4 to generate detailed descriptions. The right side of Figure 10 highlights the application of the SOTA 'Set of Mark' (SoM[†] [50]) technique to enhance the capability of GPT-4(V) in acquiring deeper knowledge. SoM involves creating masks for each object in the image using SAM, each distinguished by a unique identifier. This marked image then serves as an input for GPT-4V, enabling it to respond to queries necessitating visual grounding with greater accuracy and relevance.

4 Additional Visual Results

In Figure 6, we present additional visualization results for our approach. These results demonstrate that VATEX can successfully segment referred objects in a

[†]<https://github.com/microsoft/SoM>

variety of scenarios, including complex expressions and scenes. To further illustrate our method’s capabilities, we have also created a video demo that compares our approach to ReferFormer on Ref-Youtube-VOS. This video demo is provided as an attachment.



Fig. 6: Qualitative results of VATEX according to different language expressions for each image on the validation split of G-Ref.

References

1. Botach, A., Zheltonozhskii, E., Baskin, C., Baskin, C.: End-to-end referring video object segmentation with multimodal transformers. In: Proceedings of the IEEE/CVF Conference on Computer Vision and Pattern Recognition. pp. 4985–4995 (2022) [4](#)
2. Carion, N., Massa, F., Synnaeve, G., Usunier, N., Kirillov, A., Zagoruyko, S.: End-to-end object detection with transformers. In: Computer Vision–ECCV 2020: 16th European Conference, Glasgow, UK, August 23–28, 2020, Proceedings, Part I 16. pp. 213–229. Springer (2020) [4](#)
3. Chen, L.C., Papandreou, G., Schroff, F., Adam, H.: Rethinking atrous convolution for semantic image segmentation. arXiv preprint arXiv:1706.05587 (2017) [1](#)
4. Chen, T., Kornblith, S., Norouzi, M., Hinton, G.: A simple framework for contrastive learning of visual representations. In: Proceedings of the 37th International Conference on Machine Learning. ICML’20, JMLR.org (2020) [4](#)
5. Chen, X., Fan, H., Girshick, R.B., He, K.: Improved baselines with momentum contrastive learning. arXiv preprint arXiv:2003.04297 (2020) [4](#)
6. Cheng, B., Misra, I., Schwing, A.G., Kirillov, A., Girdhar, R.: Masked-attention mask transformer for universal image segmentation. In: Proceedings of the IEEE/CVF Conference on Computer Vision and Pattern Recognition. pp. 1290–1299 (2022) [5](#), [9](#), [17](#)
7. Cheng, B., Schwing, A.G., Kirillov, A.: Per-pixel classification is not all you need for semantic segmentation. In: NeurIPS (2021) [9](#)
8. Ding, H., Liu, C., Wang, S., Jiang, X.: Vision-language transformer and query generation for referring segmentation. In: Proceedings of the IEEE/CVF International Conference on Computer Vision. pp. 16321–16330 (2021) [4](#), [5](#), [10](#)
9. Ding, H., Liu, C., Wang, S., Jiang, X.: Vlt: Vision-language transformer and query generation for referring segmentation. IEEE Transactions on Pattern Analysis and Machine Intelligence (2022) [2](#), [4](#), [8](#), [10](#), [19](#)
10. Ding, Z., Hui, T., Huang, J., Wei, X., Han, J., Liu, S.: Language-bridged spatial-temporal interaction for referring video object segmentation. In: Proceedings of the IEEE/CVF Conference on Computer Vision and Pattern Recognition. pp. 4964–4973 (2022) [4](#)
11. Feng, G., Hu, Z., Zhang, L., Lu, H.: Encoder fusion network with co-attention embedding for referring image segmentation. In: Proceedings of the IEEE/CVF Conference on Computer Vision and Pattern Recognition. pp. 15506–15515 (2021) [2](#)
12. Feng, G., Hu, Z., Zhang, L., Lu, H.: Encoder Fusion Network with Co-Attention Embedding for Referring Image Segmentation. In: 2021 IEEE/CVF Conference on Computer Vision and Pattern Recognition (CVPR). pp. 15501–15510 (Jun 2021), iSSN: 2575-7075 [3](#)
13. He, K., Fan, H., Wu, Y., Xie, S., Girshick, R.: Momentum contrast for unsupervised visual representation learning. In: Proceedings of the IEEE/CVF Conference on Computer Vision and Pattern Recognition (CVPR). pp. 9726–9735 (06 2020) [4](#)
14. Heo, M., Hwang, S., Oh, S.W., Lee, J.Y., Kim, S.J.: Vita: Video instance segmentation via object token association. arXiv preprint arXiv:2206.04403 (2022) [1](#)
15. Hu, R., Rohrbach, M., Darrell, T.: Segmentation from natural language expressions. In: Computer Vision–ECCV 2016: 14th European Conference, Amsterdam, The Netherlands, October 11–14, 2016, Proceedings, Part I 14. pp. 108–124. Springer (2016) [3](#)

16. Huang, S., Hui, T., Liu, S., Li, G., Wei, Y., Han, J., Liu, L., Li, B.: Referring Image Segmentation via Cross-Modal Progressive Comprehension. In: 2020 IEEE/CVF Conference on Computer Vision and Pattern Recognition (CVPR). pp. 10485–10494 (Jun 2020), iSSN: 2575-7075 [3](#)
17. Huang, Z., Satoh, S.: Referring image segmentation via joint mask contextual embedding learning and progressive alignment network. In: Bouamor, H., Pino, J., Bali, K. (eds.) Proceedings of the 2023 Conference on Empirical Methods in Natural Language Processing. pp. 7753–7762. Association for Computational Linguistics, Singapore (Dec 2023) [4](#), [10](#), [17](#)
18. Kazemzadeh, S., Ordonez, V., Matten, M., Berg, T.: ReferItGame: Referring to objects in photographs of natural scenes. In: Proceedings of the 2014 Conference on Empirical Methods in Natural Language Processing (EMNLP). pp. 787–798. Association for Computational Linguistics, Doha, Qatar (Oct 2014) [10](#), [16](#)
19. Khoreva, A., Rohrbach, A., Schiele, B.: Video object segmentation with language referring expressions. In: Computer Vision—ACCV 2018: 14th Asian Conference on Computer Vision, Perth, Australia, December 2–6, 2018, Revised Selected Papers, Part IV 14. pp. 123–141. Springer (2019) [10](#), [16](#), [17](#)
20. Kim, N., Kim, D., Lan, C., Zeng, W., Kwak, S.: Restr: Convolution-free referring image segmentation using transformers. In: Proceedings of the IEEE/CVF Conference on Computer Vision and Pattern Recognition (CVPR). pp. 18145–18154 (June 2022) [23](#), [24](#)
21. Kim, S., Kang, M., Park, J.: Risclip: Referring image segmentation framework using clip. arXiv preprint arXiv:2306.08498 (2023) [21](#), [22](#)
22. Kirillov, A., Mintun, E., Ravi, N., Mao, H., Rolland, C., Gustafson, L., Xiao, T., Whitehead, S., Berg, A.C., Lo, W.Y., et al.: Segment anything. In: Proceedings of the IEEE/CVF International Conference on Computer Vision. pp. 4015–4026 (2023) [18](#), [19](#)
23. Kuhn, H.W.: The Hungarian Method for the Assignment Problem. *Naval Research Logistics Quarterly* **2**(1–2), 83–97 (March 1955) [9](#)
24. Li, M., Sigal, L.: Referring transformer: A one-step approach to multi-task visual grounding. *Advances in neural information processing systems* **34**, 19652–19664 (2021) [4](#), [18](#)
25. Li, R., Li, K., Kuo, Y.C., Shu, M., Qi, X., Shen, X., Jia, J.: Referring image segmentation via recurrent refinement networks. In: 2018 IEEE/CVF Conference on Computer Vision and Pattern Recognition. pp. 5745–5753 (2018) [2](#)
26. Li, X., Wang, J., Xu, X., Li, X., Raj, B., Lu, Y.: Towards robust referring video object segmentation with cyclic relational consensus (2023) [19](#)
27. Lin, T.Y., Dollár, P., Girshick, R., He, K., Hariharan, B., Belongie, S.: Feature pyramid networks for object detection (2017) [7](#)
28. Liu, C., Ding, H., Jiang, X.: Gres: Generalized referring expression segmentation. In: Proceedings of the IEEE/CVF Conference on Computer Vision and Pattern Recognition. pp. 23592–23601 (2023) [17](#), [21](#)
29. Liu, D., Zhang, H., Zha, Z.J., Wu, F.: Learning to Assemble Neural Module Tree Networks for Visual Grounding. In: 2019 IEEE/CVF International Conference on Computer Vision (ICCV). pp. 4672–4681 (Oct 2019), iSSN: 2380-7504 [3](#)
30. Liu, J., Ding, H., Cai, Z., Zhang, Y., Satzoda, R.K., Mahadevan, V., Manmatha, R.: Polyformer: Referring image segmentation as sequential polygon generation. In: Proceedings of the IEEE/CVF Conference on Computer Vision and Pattern Recognition. pp. 18653–18663 (2023) [2](#), [4](#), [18](#)

31. Liu, S., Li, F., Zhang, H., Yang, X., Qi, X., Su, H., Zhu, J., Zhang, L.: Dab-detr: Dynamic anchor boxes are better queries for detr. arXiv preprint arXiv:2201.12329 (2022) [4](#)
32. Liu, S., Zeng, Z., Ren, T., Li, F., Zhang, H., Yang, J., Li, C., Yang, J., Su, H., Zhu, J., et al.: Grounding dino: Marrying dino with grounded pre-training for open-set object detection. arXiv preprint arXiv:2303.05499 (2023) [18](#), [19](#)
33. Liu, Z., Ning, J., Cao, Y., Wei, Y., Zhang, Z., Lin, S., Hu, H.: Video swin transformer. In: Proceedings of the IEEE/CVF conference on computer vision and pattern recognition. pp. 3202–3211 (2022) [19](#)
34. Loshchilov, I., Hutter, F.: Decoupled weight decay regularization. In: International Conference on Learning Representations (2017) [16](#)
35. Luo, G., Zhou, Y., Ji, R., Sun, X., Su, J., Lin, C.W., Tian, Q.: Cascade grouped attention network for referring expression segmentation. Proceedings of the 28th ACM International Conference on Multimedia (2020) [2](#)
36. Mao, J., Huang, J., Toshev, A., Camburu, O., Yuille, A., Murphy, K.: Generation and comprehension of unambiguous object descriptions. In: 2016 IEEE Conference on Computer Vision and Pattern Recognition (CVPR). pp. 11–20 (2016) [10](#), [16](#)
37. Oord, A.v.d., Li, Y., Vinyals, O.: Representation learning with contrastive predictive coding. arXiv preprint arXiv:1807.03748 (2018) [9](#)
38. Radford, A., Kim, J.W., Hallacy, C., Ramesh, A., Goh, G., Agarwal, S., Sastry, G., Askell, A., Mishkin, P., Clark, J., et al.: Learning transferable visual models from natural language supervision. In: International conference on machine learning. pp. 8748–8763. PMLR (2021) [2](#), [4](#), [5](#)
39. Seo, S., Lee, J.Y., Han, B.: Urvos: Unified referring video object segmentation network with a large-scale benchmark. In: Computer Vision–ECCV 2020: 16th European Conference, Glasgow, UK, August 23–28, 2020, Proceedings, Part XV 16. pp. 208–223. Springer (2020) [10](#), [16](#)
40. Su, W., Miao, P., Dou, H., Wang, G., Qiao, L., Li, Z., Li, X.: Language adaptive weight generation for multi-task visual grounding. In: Proceedings of the IEEE/CVF Conference on Computer Vision and Pattern Recognition. pp. 10857–10866 (2023) [3](#), [4](#), [10](#), [21](#), [22](#)
41. Tang, J., Zheng, G., Shi, C., Yang, S.: Contrastive grouping with transformer for referring image segmentation. In: Proceedings of the IEEE/CVF Conference on Computer Vision and Pattern Recognition. pp. 23570–23580 (2023) [17](#)
42. Wang, W., Xie, E., Li, X., Fan, D.P., Song, K., Liang, D., Lu, T., Luo, P., Shao, L.: Pyramid vision transformer: A versatile backbone for dense prediction without convolutions. In: Proceedings of the IEEE/CVF international conference on computer vision. pp. 568–578 (2021) [1](#)
43. Wang, W., Liu, J., He, X., Zhang, Y., Chen, C., Shen, J., Zhang, Y., Li, J.: Cm-masked: Cross-modality masked self-distillation for referring image segmentation. arXiv preprint arXiv:2305.11481 (2023) [10](#), [22](#)
44. Wang, Y., Xu, Z., Wang, X., Shen, C., Cheng, B., Shen, H., Xia, H.: End-to-end video instance segmentation with transformers. In: Proceedings of the IEEE/CVF conference on computer vision and pattern recognition. pp. 8741–8750 (2021) [1](#)
45. Wang, Z., Lu, Y., Li, Q., Tao, X., Guo, Y., Gong, M., Liu, T.: Cris: Clip-driven referring image segmentation. In: Proceedings of the IEEE/CVF conference on computer vision and pattern recognition. pp. 11686–11695 (2022) [4](#), [8](#), [10](#), [17](#), [21](#), [22](#)
46. Wu, J., Jiang, Y., Sun, P., Yuan, Z., Luo, P.: Language as queries for referring video object segmentation. In: Proceedings of the IEEE/CVF Conference on Computer Vision and Pattern Recognition. pp. 4974–4984 (2022) [4](#), [5](#), [10](#), [11](#), [17](#), [19](#)

47. Wu, J., Liu, Q., Jiang, Y., Bai, S., Yuille, A., Bai, X.: In defense of online models for video instance segmentation. In: Computer Vision–ECCV 2022: 17th European Conference, Tel Aviv, Israel, October 23–27, 2022, Proceedings, Part XXVIII. pp. 588–605. Springer (2022) [1](#)
48. Wu, Z., Xiong, Y., Yu, S.X., Lin, D.: Unsupervised feature learning via non-parametric instance discrimination. In: 2018 IEEE/CVF Conference on Computer Vision and Pattern Recognition. pp. 3733–3742 (2018) [4](#)
49. Xie, E., Wang, W., Yu, Z., Anandkumar, A., Alvarez, J.M., Luo, P.: Segformer: Simple and efficient design for semantic segmentation with transformers. *Advances in Neural Information Processing Systems* **34**, 12077–12090 (2021) [1](#)
50. Yang, J., Zhang, H., Li, F., Zou, X., Li, C., Gao, J.: Set-of-mark prompting unleashes extraordinary visual grounding in gpt-4v. *arXiv preprint arXiv:2310.11441* (2023) [25](#)
51. Yang, S., Wang, X., Li, Y., Fang, Y., Fang, J., Liu, W., Zhao, X., Shan, Y.: Temporally efficient vision transformer for video instance segmentation. In: Proceedings of the IEEE/CVF Conference on Computer Vision and Pattern Recognition. pp. 2885–2895 (2022) [1](#)
52. Yang, Z., Wang, J., Tang, Y., Chen, K., Zhao, H., Torr, P.H.: Lavt: Language-aware vision transformer for referring image segmentation. In: Proceedings of the IEEE/CVF Conference on Computer Vision and Pattern Recognition. pp. 18155–18165 (2022) [2](#), [3](#), [4](#), [10](#), [17](#), [22](#)
53. Ye, L., Rochan, M., Liu, Z., Wang, Y.: Cross-modal self-attention network for referring image segmentation. In: Proceedings of the IEEE/CVF conference on computer vision and pattern recognition. pp. 10502–10511 (2019) [2](#)
54. Zhou, K., Yang, J., Loy, C.C., Liu, Z.: Learning to prompt for vision-language models. *International Journal of Computer Vision* (2022) [6](#)
55. Zhu, C., Zhou, Y., Shen, Y., Luo, G., Pan, X., Lin, M., Chen, C., Cao, L., Sun, X., Ji, R.: Seqtr: A simple yet universal network for visual grounding. In: European Conference on Computer Vision. pp. 598–615. Springer (2022) [4](#), [18](#)
56. Zhu, X., Su, W., Lu, L., Li, B., Wang, X., Dai, J.: Deformable detr: Deformable transformers for end-to-end object detection. *arXiv preprint arXiv:2010.04159* (2020) [4](#)
57. Zou*, X., Dou*, Z.Y., Yang*, J., Gan, Z., Li, L., Li, C., Dai, X., Wang, J., Yuan, L., Peng, N., Wang, L., Lee*, Y.J., Gao*, J.: Generalized decoding for pixel, image and language (2022) [18](#), [19](#)
58. Zou, X., Yang, J., Zhang, H., Li, F., Li, L., Wang, J., Wang, L., Gao, J., Lee, Y.J.: Segment everything everywhere all at once. *Advances in Neural Information Processing Systems* **36** (2024) [18](#), [19](#)